PNAS RESEARCH ARTICLE | ENGINEERING

Scalable networks of multimodal haptic arrays for plantar sensory substitution

Matthew T. Flavin[a,b,1,2], Yu-Ting Huang[b,c,2], Dimitrios Simatos[b,2], Rui Hua[d,e,f,2], Shreya Aalla[d,2], Jesse Cornman[g], Richa Rai[d], Jihun Park[b], Chinmay Bandapalli[a], Tara Saxena[c], Molly Henry[d], Joseph Harris[d], Kelly L. Breen[d], Jacob Trueb[b], Raden Schell[a], Sam A. Allahverdi[a], Fatimah Al-Najjar[c], Jae-Young Yoo[b,h], Aadeel Akhtar[g], Arun Jayaraman[d,i,1], and John A. Rogers[b,c,j,k,l,1]

Affiliations are included on p. 9.

Contributed by John A. Rogers; received December 20, 2025; accepted May 6, 2026; reviewed by Luigi G. Occhipinti and Huiliang Wang

Feet provide essential sensory input, supporting body awareness for safe movement. The impairment of plantar sensation, arising in conditions such as stroke and spinal cord injury, has a major impact on mobility, balance, and quality of life. Substituting the sensation of plantar pressure to another area on the body with intact somatosensory abilities requires capabilities for fast, programmable delivery of haptic feedback. Here, we introduce a wireless network of skin-conformable, multimodal haptic arrays that deliver high-density thermal and vibrotactile patterns anywhere on the body. Central to this approach is a hybrid motor unit that independently controls thermal and mechanical stimulation, enabling 128 degrees of freedom across 64 addressable nodes. Electromechanical characterization establishes precise, simultaneous, and safe modulation of both modalities. Psychophysical experiments demonstrate reliable spatial discrimination of colocated heat and vibration. These haptic arrays form the receivers in a sensory substitution system that delivers patterns of vibrotactile stimulation to mirror the distribution of pressure recorded from an insole-based array of pressure sensors. Exploratory case studies in individuals with spinal cord injury and stroke demonstrate feasibility and suggest improved performance during standing balance and walking tests. Altogether, this work highlights the potential of information-rich cutaneous interfaces to substitute plantar sensation, expanding the scope of somatosensory engagement for rehabilitation, entertainment, and education.

wearable electronics | haptics | rehabilitation

Significance

The sense of touch in our feet is essential for safe movement, and its impairment in conditions such as stroke and spinal cord injury contributes to diminished quality of life. Substituting missing foot sensation requires not only sensors for reading that information but also a nonintrusive means to display it in real time. This article demonstrates a system of wireless, skin-conformable haptic arrays. A hybrid motor unit addresses long-standing challenges in the integration of high-resolution, multimodal haptics, delivering precise patterns of heat and vibration and giving the user more information about their physical environment. Systematic human perception experiments and case studies with sensory-impaired individuals establish foundational principles, raising implications for sensory symptoms affecting a large portion of the global population.

The feet provide a major source of somatosensory information about body–environment interactions during standing and walking. Somatosensory feedback is essential for balance control and functional mobility, both of which support activities of daily living. Individuals with sensory impairments often report barriers to participation in leisure activities and employment (1). Impairment of cutaneous plantar sensation may disrupt balance, contribute to abnormal gait patterns, and increase the risk of falls (2). Deficits in plantar sensation and associated mobility challenges are common in individuals with chronic neurological conditions, such as stroke and spinal cord injury (SCI) (3, 4). They are also associated with reduced mobility, decreased quality of life, and increased caregiver burden. Rehabilitative interventions traditionally prioritize motor impairments, while sensory deficits, though impactful on functional outcomes, are often unassessed and therefore undertreated (5). This gap motivates the development of new enabling technologies that compensate for impaired sensory input.

Individuals with stroke and SCI often exhibit both motor and sensory impairments that result in compensatory strategies which result in abnormal, unsafe gait patterns and increased fall risk (2, 6). In supervised clinical settings, clinicians provide feedback to promote safer and more efficient gait mechanics (7, 8). However, outside of these structured environments, individuals rely on self-selected or impairment-driven movement strategies during activities of daily living, reinforcing maladaptive compensations. As a result, there remains a need for tools that can deliver real-time sensorimotor feedback to patients during activities of daily living outside of supervised clinical settings (9, 10).

One commonly adopted compensatory strategy for diminished plantar sensation is increased reliance on visual input to perceive spatial cues and regular gait (11, 12). Although visual compensation can be effective in structured or familiar environments, its utility (13) is variable and can substantially increase cognitive demands during complex real-world tasks. In environments that require continuous visual monitoring for safety, such as navigating crowds or crossing streets, reliance on vision alone for gait control may be impractical or insufficient. Consistent with this, one participant in this study reports ambulating independently within the home environment, but relying on a wheelchair in public, citing the need to allocate visual attention to environmental scanning rather than monitoring foot placement.

Reviewers: L.G.O., University of Cambridge; and H.W., The University of Texas at Austin.

Competing interest statement: J. Rogers and one reviewer were co-authors on a review article published in 2023. The authors declare no other competing interests.

[1]To whom correspondence may be addressed. Email: mflavin@gatech.edu, a-jayaraman@northwestern.edu, or jrogers@northwestern.edu.

[2]M.T.F., Y.-T.H., D.S., R.H., and S.A. contributed equally to this work.

This article contains supporting information online at https://www.pnas.org/lookup/suppl/doi:10.1073/pnas.2536577123/-/DCSupplemental.

Published June 15, 2026.

To address limitations of vision-based compensation during functional mobility, sensory substitution approaches have increasingly explored nonvisual feedback channels. In this work, the authors demonstrate a wearable system designed to support compensation for impaired plantar sensation without relying on vision. This sensory substitution approach conveys missing plantar sensory input through tactile feedback delivered to a body segment with intact somatosensation, providing nonvisual sensorimotor support during unsupervised gait.

We focus on cutaneous feedback as a means of substituting information typically conveyed through plantar sensation, as the skin is capable of conveying spatially organized sensory information (14). Cutaneous receptors, such as thermoreceptors and mechanoreceptors illustrated in Fig. 1*A*, provide distinct, independent sensory channels, all of which are critical for perceiving the physical environment (15–17). The introduction of wearable haptic devices, leveraging electrotactile (18, 19), electrostatic (20, 21), pneumatic (22, 23), and electromagnetic (24–27) mechanisms, offers powerful opportunities for interfacing with mechanoreceptors distributed across the surface of the skin. Similarly, thermal augmented reality systems—based on thermoelectric heating and cooling—are capable of reproducing patterns of temperature across the skin (28, 29). Although somatosensory feedback represents an emerging frontier in augmented and virtual reality (AR/VR) research (30), long-standing challenges exist in creating low-profile, energy-efficient electronic components capable of thermal and mechanical actuation (Fig. 1*B*). Here, we address these challenges in selectively engaging somatosensory channels with high spatial resolution from untethered, wearable devices (Fig. 1*C*). Central to our approach is a hybrid direct-current (DC) motor strategy that enables 128 degrees of freedom across 64 independently controlled haptic units.

Another limitation of existing haptic wearables is that they tend to fixate on specific body segments, such as the hands (22, 31, 32), while ignoring sensory experiences distributed across the skin as a whole. For assistive and augmentative applications, glove-based systems risk burdening users by impairing the normal abilities of their hands (33). Solving these limitations, this paper demonstrates a wireless network of dual skin-conformable haptic arrays with adaptive mechanical features that offer a generalizable interface to our somatosensory receptors (Fig. 1*C*). These capabilities support flexible, lightweight, interconnected devices with functional diversity that exceeds previous reports (*SI Appendix*, Table S1) (26, 28, 34–36). Electromechanical characterization and psychophysical studies validate independent control and perception of thermal and mechanical cues across the array.

When deployed as a skin-conformable interface for sensory substitution, plantar pressure distributions derived from insole-based sensors map onto these arrays to convey missing plantar information (Fig. 1*D*). Using principles well aligned with existing plantar sensory substitution strategies (*SI Appendix*, Table S2) (37–40), our approach expands beyond single-modality implementations at fixed body segments. Preserving an untethered form factor suitable for daily use, exploratory case studies in individuals with SCI and stroke demonstrate feasibility of vibrotactile feedback and suggest improved task performance. Ultimately, this study highlights the potential of comprehensively engaging cutaneous senses with spatially patterned, multimodal stimuli to support functional mobility in populations with plantar sensory impairment, broadly including age-related sensory decline (41), amputation (42, 43), and peripheral neuropathy (44).

Results

Spatiotemporal Control of Heat and Vibration. Our system delivers multisensory actuation at scale: 64 spatial locations stimulate concurrently over two devices, with 128 total degrees

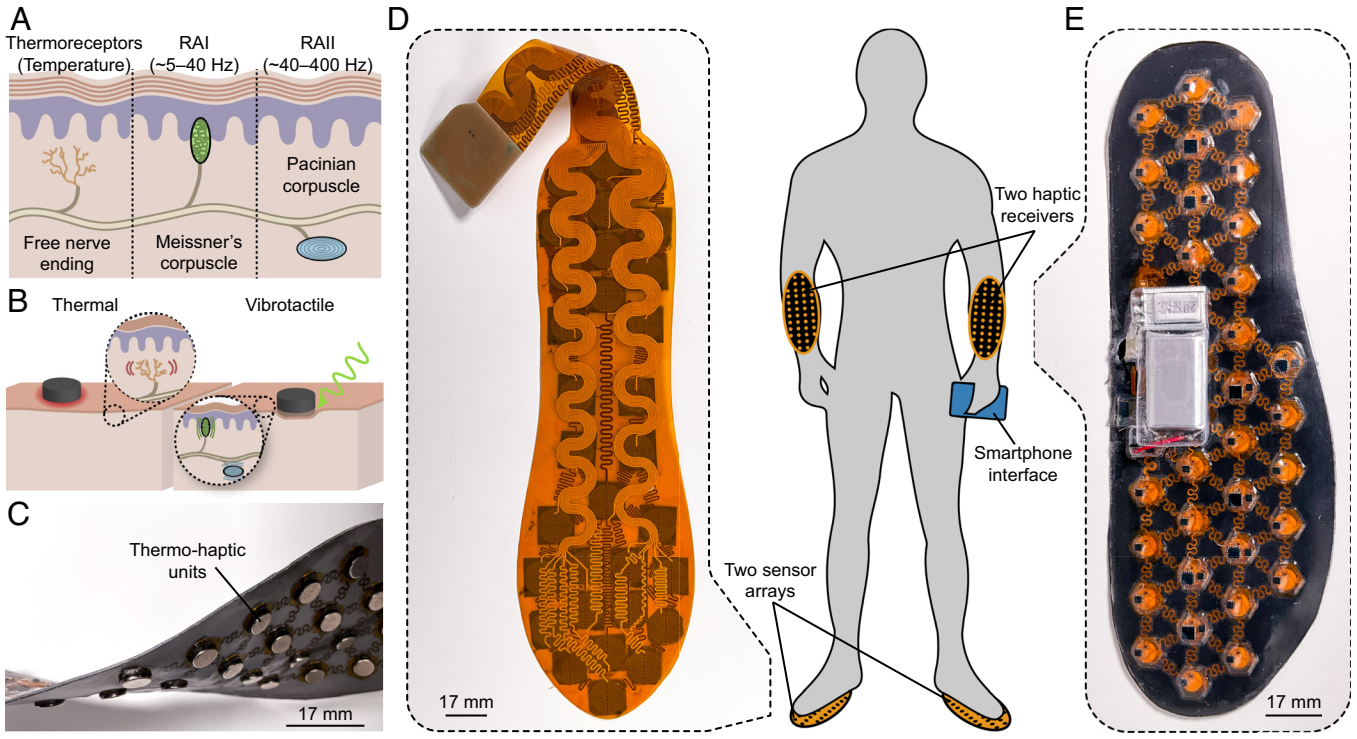

Fig. 1. Multisensory feedback with a wireless, battery-powered array of haptic actuators. (*A*) Illustration of skin thermoreceptors and mechanoreceptors (RA, rapidly adapting frequency response). (*B*) Modes of cutaneous stimulation, illustrating targeted mechanoreceptors and thermoreceptors. (*C*) Photograph of the skin-conformable array of thermo-haptic units. (*D* and *E*) Key elements of the plantar sensory substitution system. (*D*) Insole-based pressure sensor array. (*E*) Forearm-mounted array of thermo-haptic motor units.

of freedom arising from independently addressable thermal and vibrotactile channels. Patterns of stimuli can be prescribed to match useful sensory data, such as the distribution of pressure sensed by the foot during walking. Each actuation unit is organized as a node arranged in a hexagonal tiling and linked through stretchable serpentine interconnects. A soft, silicone-based encapsulation forms a compliant, skin-facing barrier that supports close mechanical coupling during repeated placement and extended wear. Thus, the device can flex and bend, accommodating curved areas of the body such as the forearms.

Each motor unit, an eccentric rotating mass (ERM) actuator, delivers both mechanical and thermal stimulation (Fig. 2*A*). Independent control of these modalities follows from a bipolar waveform in which the positive half-cycle sets the vibrotactile amplitude while the negative half-cycle applies active braking to the DC motor (Fig. 2*B*). This braking phase cancels net angular momentum and increases resistive dissipation within the actuator, thereby producing heat according to Joule's law. With a closely coupled temperature sensor, the resistive heating of the actuator is controlled through a proportional–integral–derivative (PID) algorithm operating on the microcontroller embedded in the array. This allows the user to prescribe temperature setpoints for thermal feedback. Fig. 3 *A* and *B* show the device responding correctly to given setpoints. The PID controller maintains safety temperature limits across all modes of operation, including vibration.

The independent control of heat and vibration is demonstrated using accelerometer measurements and absolute temperature readings. As shown in Fig. 3*C*, increasing the temperature setpoint causes minimal changes in vibration amplitude. At the same time, heat delivery alone (0% vibration setpoint) does not result in detectable vibration (see *SI Appendix*, Fig. S1 for frequency-domain analysis). For t = 15 s and t = 35 s, we see that the gradient is parallel to the axis of increasing vibration. At t = 55 s, the prescribed temperature acts as the safety limits of the actuator—for lower setpoints, 30~35 °C, the vibration is automatically throttled despite increasing prescribed vibration. In Fig. 3*D*, we see how the temperatures of the actuators respond under varying vibration and temperature setpoints. As intended, the gradient of increasing temperature is

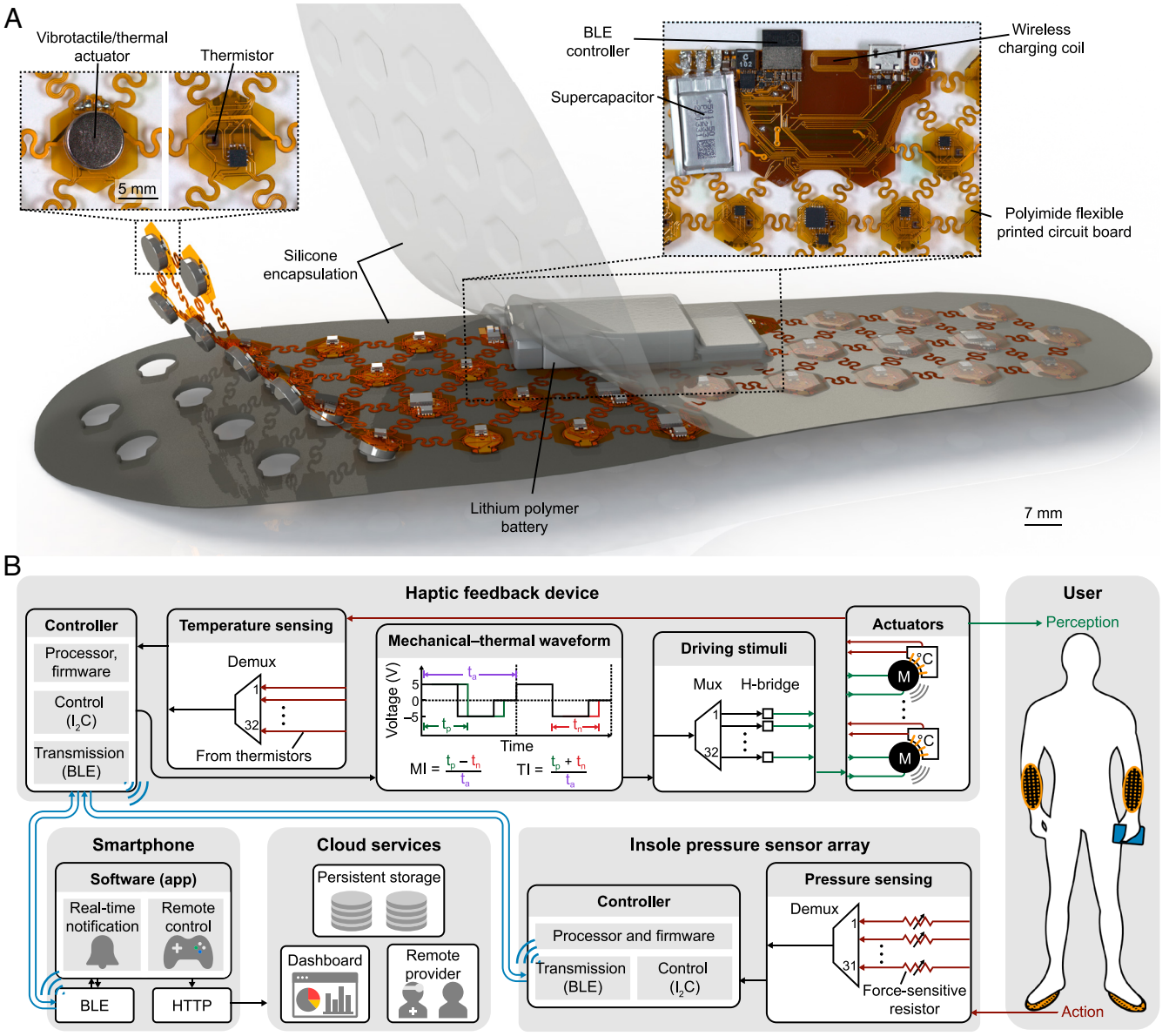

Fig. 2. Wireless, battery-powered operation of an array of actuator units capable of both mechanical and thermal stimulation. (*A*) 3D illustration and photographs of the haptic array showing key elements. (*B*) Block diagram showing closed loop operation of the sensory substitution system, orchestrated by the haptic array (MI, mechanical intensity; TI, thermal intensity; BLE, Bluetooth Low Energy).

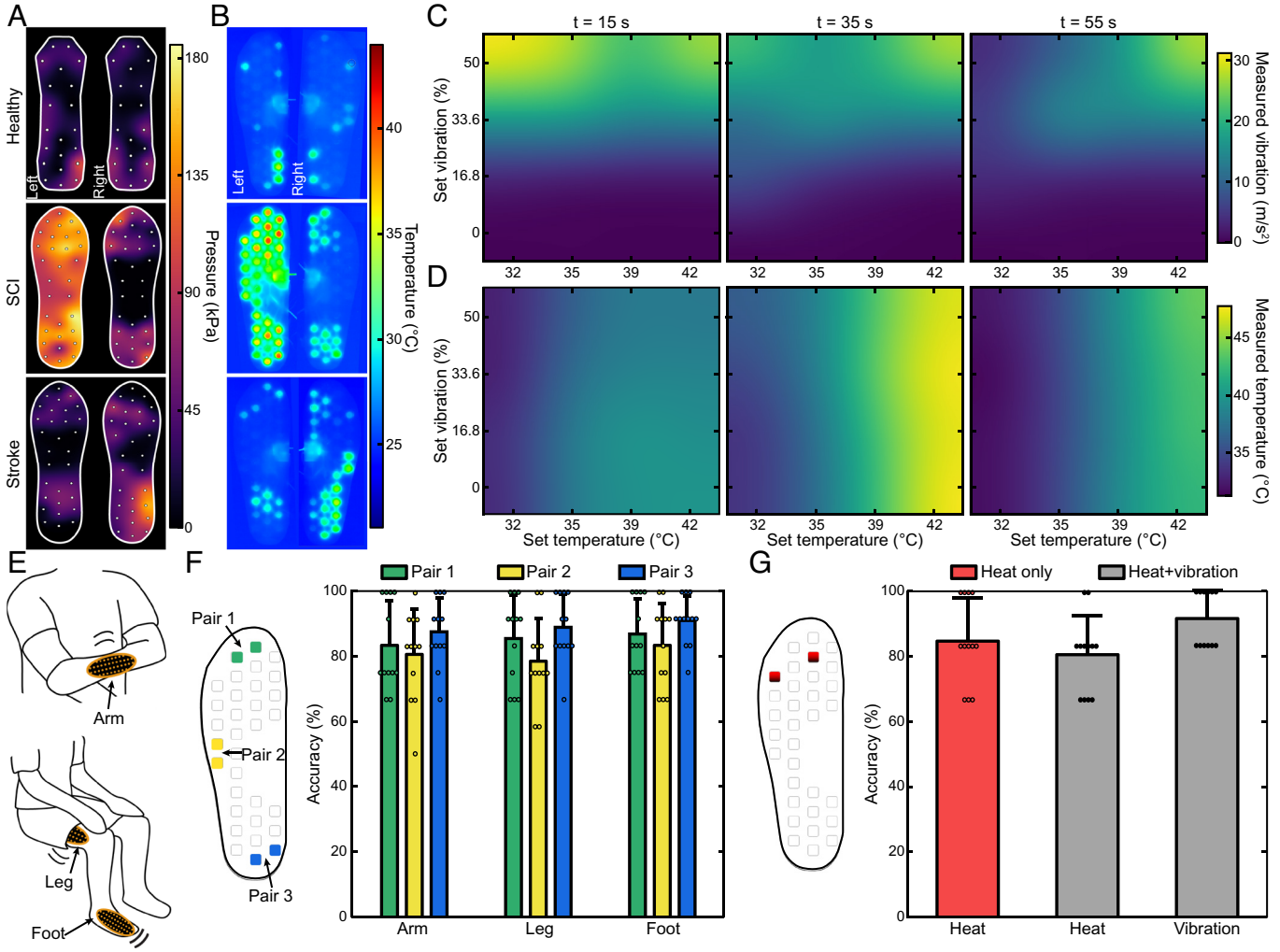

Fig. 3. Evaluating the performance and perception of hybrid thermal–mechanical operation. (*A* and *B*) Replaying patterns of activity recorded in human experiments for a healthy participant (small insole variation), SCI participant (Participant P4; large insole variation), and stroke participant (Participant P5; large insole variation). (*A*) Pressure distributions measured during clinical sessions. (*B*) Thermal images of the haptic array delivering heat to match the recorded pressure, averaged over 5 min. (*C* and *D*) Mechanical and thermal characterization of a unit actuator during prescribed combinations of temperature and vibration setpoints, demonstrating the independence between these two axes. The axes correspond to stimuli setpoints. (*C*) Colormaps of measured vibration resulting from the given setpoints at t = 15, 35, and 55 s from stimuli onset (accelerometer sampling at 1.666 kHz). (*D*) Colormaps of measured temperature resulting from the given setpoints at t = 15, 35, and 55 s from stimuli onset (thermal camera). (*E*–*G*) Odd-man-out forced choice psychophysical assessment of heat and vibration on healthy human participants (n = 12, 6 male, 6 female, ages 28 to 34; bars, mean; circle markers, individual trial results; whiskers, standard deviation). For both experiments, $P < 0.0012$ (Wilcoxon signed-rank test, H_0: random selection between three choices). (*E*) Illustration of body locations assessed. (*F*) Accuracy of participant answers for vibration stimuli. The illustration shows three pairs of locations on the device that were tested. (*G*) Accuracy of participant answers for heat stimuli, delivered alone, and heat + vibration stimuli, delivered at the same time.

parallel to the temperature axis, and vibration alone (32 °C temperature setpoint) does not increase temperature. Together, these features enable precise, simultaneous, and safe modulation of heat and vibration from a single ERM unit within the array.

All actuation and sensing are coordinated by a system-on-chip microcontroller (Fig. 2*A*). Each haptic node interfaces with the microcontroller through serial and general-purpose input–output (GPIO) channels. Analog multiplexers and GPIO expanders reduce the number of traces leading to the microprocessor, allowing thinner, more compliant interconnects between nodes. Real-time, bidirectional data flow, coordinated by the embedded firmware visualized in Fig. 2*B*, continuously returns temperature from all 32 addressable locations. Bluetooth Low Energy (BLE) links two haptic receivers, enabling 64 addressable locations in the studied configuration. As shown in Fig. 2*B*, BLE also connects the haptic receivers to the pressure-sensing insoles and the smartphone interface, which remotely monitor and configure the system. The smartphone software also relays clinical and operational metadata to the cloud for persistent storage and remote review, allowing each session to be logged alongside task annotations and synchronized sensor measurements for later analysis.

As shown in *SI Appendix*, Fig. S2, one array of 32 actuators consumes 0.62 W under the characteristic load corresponding to the pressure reported for Participant P4 in Fig. 3*A*. When the device is only communicating between the insole and smartphone over BLE, the device draws 0.09 W. With a 500-mAh battery, these conditions support active use of the device under highest intensity for 3 h. As shown in *SI Appendix*, Fig. S2, using a 12.5% max duty cycle may allow the device to operate for as long as 7 h.

Participant Perception of Heat and Vibration. Not only can the system control the vibration across each location in the array, but users can feel adjacent locations independently. Fig. 3*E* outlines the setup of an odd-man-out spatial discrimination task that

asks participants to consider three vibrations (50% duty cycle intensity for 3 s) successively delivered to two adjacent actuator locations. As shown in Fig. 3*F* and *SI Appendix*, Tables S4–S6, the participants successfully indicate which actuator location was different from the other two with an overall accuracy of 84.9% (P = 0.0011, Wilcoxon signed-rank test, H_0: random selection between three choices; *SI Appendix*, Table S9). Pairs of adjacent actuators were chosen in three distinct regions of the haptic device, each showing similar performances. The pair mounted on the distal end of the device (Pair 1), corresponding to the toes in the sensory substitution system, yields an accuracy of 85.2%. The pair mounted on middle of the device (Pair 2), corresponding to the arch in the sensory substitution system, yields an accuracy of 80.8%. The pair mounted on proximal end of the forearm (Pair 3), corresponding to the heel in the sensory substitution system, yields an accuracy of 89.1%. As shown in Fig. 3*F*, the devices yield similar overall performance when tested on the leg, arm, and foot of each participant.

Our system aims to deliver heat and dynamic vibration as perceptually distinct channels of information. Fig. 3*G* details another odd-man-out experiment that evaluates patterns of heat applied at 40 °C for 20 s. For a pair of nodes spaced 27 mm apart in the toe area, participants correctly chose the differing location with an accuracy of 84.7% ($P < 0.001$, Wilcoxon signed-rank test, H_0: random selection between three choices; *SI Appendix*, Table S9). We then performed a simultaneous odd-man-out experiment that studies joint perception of heat and vibration (spaced at 27 mm). On each trial, a 20 s heat stimulus is followed by a 3 s vibrotactile stimulus during the actuator's cooling phase, with one "odd" location per modality presented in randomized order. Participants identify the odd location for both modalities with an accuracy of 86.1% (Fig. 3*G* and *SI Appendix*, Tables S7 and S8), demonstrating that colocated thermal and vibrotactile cues generated by the hybrid actuator remain perceptually separable even when presented together.

Pattern Matching Between Feet and Forearms. In the sensory substitution system schematically illustrated in Fig. 4*A*, the haptic arrays connect wirelessly to pressure sensors embedded in flexible insoles. The insoles sit inside the shoes and continuously record the missing sensory information—plantar pressure—which is streamed in real time over BLE to the forearm-mounted haptic arrays.

To assess whether users intuitively map vibrotactile patterns on the forearm to locations on the foot and vice versa, we evaluate a pattern-matching task in cohorts of individuals with intact sensation (described herein as "healthy individuals"), with stroke, and with SCI. As shown in Figs. 4 *B* and *C*, we test discrete locations on the foot for matching accuracy. For each location, participants first load the prescribed region of the foot while the insole records a pressure snapshot that serves as the reference pattern. During the matching phase, these snapshots replay in random order through the haptic device. Participants then indicate the perceived foot location by pointing to the schematic in Fig. 4*B* and by reproducing the corresponding pressure distribution.

Healthy adults (n = 12; 6 male, 6 female; ages 28 to 34) demonstrate high accuracy in perceiving and replicating the reference foot pressure patterns, achieving a mean accuracy of 86.9% (Fig. 4*D*; $P < 0.001$, Wilcoxon signed-rank test, H_0: random selection between five choices; *SI Appendix*, Table S10). Accuracy is higher on the right foot (91.7%) than the left (82.0%), consistent with lateral dominance in this predominantly right-handed cohort. Across all trials, participants exhibit the greatest precision in differentiating cues presented along the vertical axis of the foot, accurately distinguishing between the toe, arch, and heel regions (toe: 95.8% left, 98.3% right; arch: 86.7% left, 93.3% right; heel: 96.7% left, 97.5% right).

Clinical participants (n = 8; 4 male, 4 female; ages 35 to 65) with lower-limb sensory impairments due to stroke (n = 1) or SCI (n = 7) show reduced accuracy and increased variability across plantar regions. Five participants use ankle-foot orthoses (AFOs) to support foot stability during daily activities, and two wore these during the tasks (*SI Appendix*, Table S3). As shown in Fig. 4*E*, mean accuracy across all trials is 56.3%, with 58.7% as the overall mean accuracy for the impaired foot and 54.3% as that for the dominant foot (n = 7; P = 0.009, Wilcoxon signed-rank test, H_0: random selection between five choices; *SI Appendix*, Table S10). Accuracy is highest for the toe region (83.3% impaired, 85.7% dominant), intermediate for the heel (73.3% impaired, 71.4% dominant), and lowest for the arch (56.7% impaired, 57.1% dominant).

One of the most notable differences between healthy and impaired participants arises from the pressure maps recorded during the task. As shown in Figs. 4 *F* and *G* and *SI Appendix*, Figs. S3–S5, the pressure snapshots recorded for different target locations cluster more tightly, yielding a smaller mean distance between reference centers-of-pressure (CoPs) and making spatial discrimination substantially more challenging. Matching accuracy follows the general trend displayed in Fig. 4*H*, increasing with larger minimum distances between reference CoPs. Because this is a dual task that requires participants to balance and support their weight on parallel bars, the reduced separability is likely influenced by their functional abilities, as quantified by the Berg Balance Scale—as shown in *SI Appendix*, Table S3, scores range from 6 to 50. Taken together, these findings indicate that coarse spatial discrimination (e.g., heel vs. toe) is largely preserved in clinical participants, but fine-grained reproduction (e.g., medial heel vs. lateral heel) of target plantar pressure distributions is impaired, leading to less distinct pressure patterns compared with healthy adults.

Piloting Real-Time Haptic Feedback During Standing and Walking. The sensor insoles and haptic receivers form a sensory substitution system that is configured on demand through the smartphone interface shown in Fig. 5*A*. This wireless, battery-operated platform functions during the normal movements of the users. Two haptic receivers, the insole-shaped arrays of embedded actuators, attach to the forearms with textile sleeves. In real-time, the patterns of pressure recorded from each of the insole-based pressure sensor arrays transmit to the haptic receivers, delivering matching patterns of vibration to the forearms. To evaluate the feasibility and usability of this system, we conduct a series of exploratory case studies assessing performance during standing balance and walking tests.

When applied during the Romberg test, shown in Fig. 5*B* and Movie S1, haptic feedback is designed to enhance postural stability by substituting somatosensory input. As shown in Fig. 5*C* and *SI Appendix*, Fig. S6, consistent improvements are observed across all participants (n = 4; 1 male, 3 females; ages 37 to 66), with balance duration increasing from 24, 9, 11, and 37 s without feedback to 48, 20, 12, and 53 s with feedback (*SI Appendix*, Fig. S6). Statistical analysis confirms a significant effect of haptic feedback on performance (P = 0.004, linear mixed model; H_0: no difference with feedback; *SI Appendix*, Table S11). On average, participants maintain balance for 9 to 122% longer when assisted by the haptic device, indicating that externally delivered cues can effectively support postural control for this group. These results provide early evidence of functional improvements for stroke and SCI participants during standing balance.

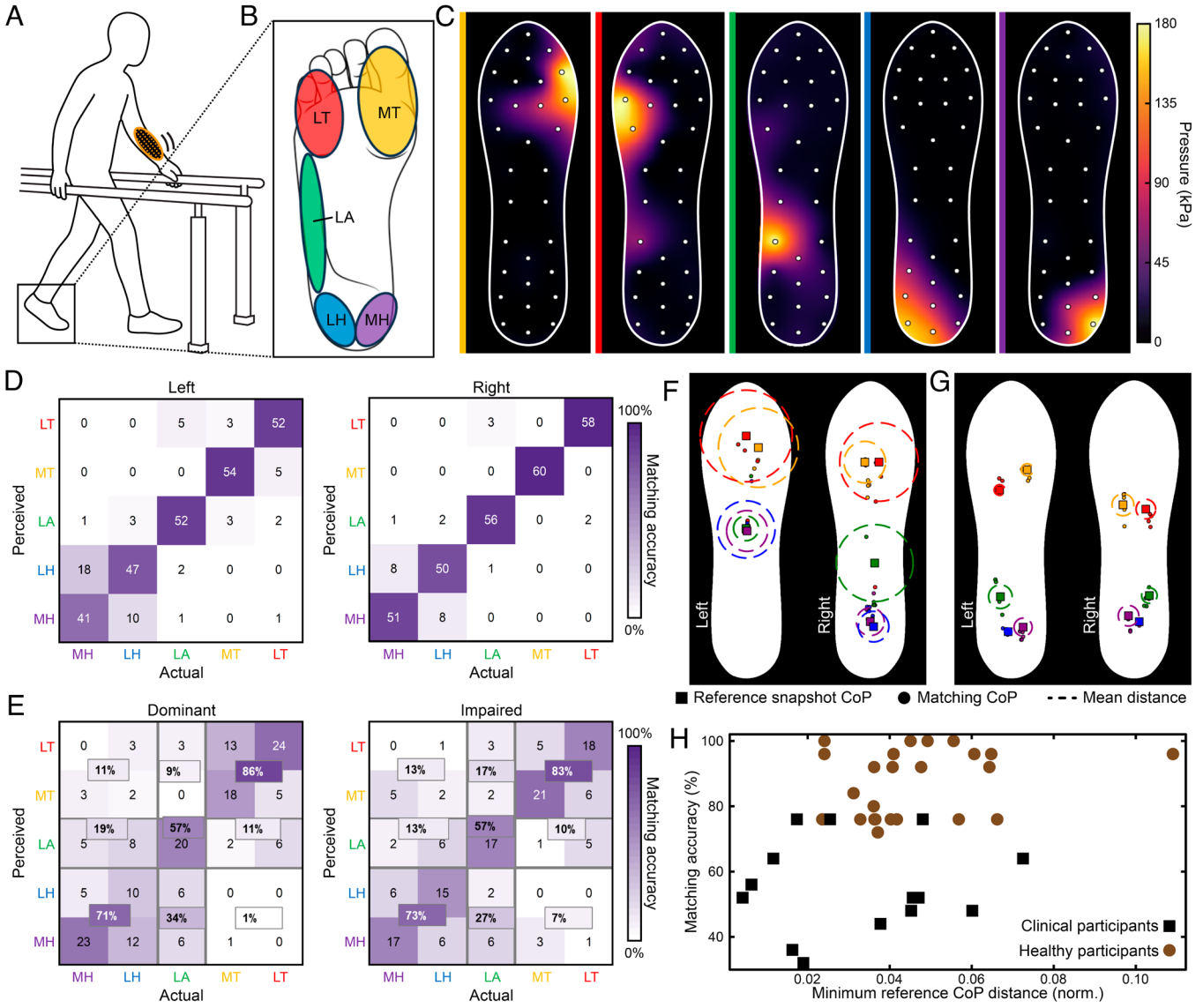

Fig. 4. Pattern matching experiments on healthy participants, SCI participants, and stroke participants. In this experiment, the participants are provided a feedback cue from the haptic device and instructed to match that pattern to a pressure distribution measured from the sensor array. (*A*) Illustration of the experimental setup used for evaluating the ability of each participant to match plantar pressure to vibration cues. (*B*) Target patterns for haptic cues (LT, lateral toes; MT, medial toes; LA, lateral arch; LH, lateral heel; MH, medial heel). (*C*) Example snapshot reference patterns. (*D*) Confusion matrix of healthy participant performance on task on the left and right sides (n = 12, 6 male, 6 female, ages 28 to 34; $P < 0.0011$, Wilcoxon signed-rank test, H_0: random selection between five choices). (*E*) Confusion matrix of clinical participant (n = 8; 4 male, 4 female; ages 35 to 65) performance on task for the side primarily affected by impairment and dominant sides (n = 7; P = 0.009, Wilcoxon signed-rank test, H_0: random selection between five choices). (*F* and *G*) Center of pressure (CoP) analysis of insole pressure data recorded during pattern matching task (square markers, CoP of each reference snapshot; circles markers, individual trial CoP; dashed circle, mean distances from trial CoPs to the actual reference CoP). The colors correspond to the corresponding reference the participant was asked to reproduce. (*F*) Example results from Participant P4. (*G*) Example results from a healthy participant (male, age 25). (*H*) Average accuracy from SCI participants and healthy participants on pattern matching as a function of minimum distance between any two reference zones for a given foot (distance normalized to insole sensor length).

Another case study of this system, reported in Fig. 5 *D–G* and *SI Appendix*, Fig. S7, evaluates feedback delivered during a 10MWT. Participant P5, who is recovering from stroke, displays toe drag during walking (male, age 58). With their eyes closed for the entire walk, they were instructed to use the real-time pressure feedback to assess how much they were favoring one side of their body. We performed motion pose analysis across 22 walks with and without feedback (Movie S2). As shown in Fig. 5*F*, feedback reduced sway with a significant 24% mean reduction in lateral standard deviation (P = 0.049, Mann–Whitney U test; H_0: no difference with feedback; *SI Appendix*, Table S12). Feedback also reduced lateral range of path deviation by 16.2%, although this effect was not statistically significant (Fig. 5*G*). The devices successfully delivered feedback during this run, and pressure data transmitted to a cloud server during this study is shown in *SI Appendix*, Fig. S8.

Discussion

Although AR/VR headsets are effective at reproducing a realistic sense of hearing and vision, current haptic interfaces are not capable of engaging the somatosensory system nearly as comprehensively as experienced in natural environments. Here, we present a platform that delivers coordinated mechanical and thermal stimulation over wide areas of the skin (116 cm^2 for every array), providing a limb-spanning interface for somatosensory engagement. This approach

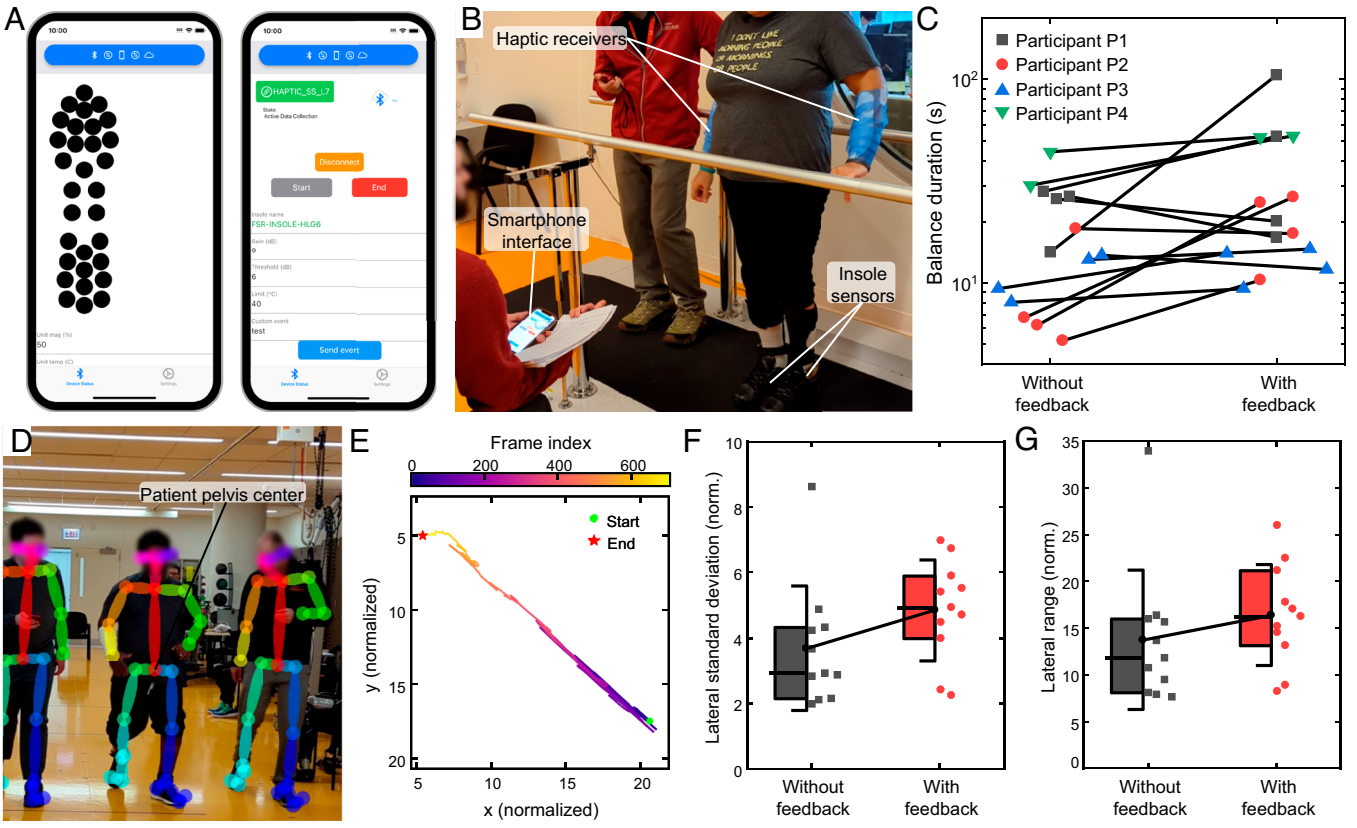

Fig. 5. Outcomes from focus group of stroke and SCI participants. (*A*) Screenshot of the smartphone interface during data collection. (*B*) Photograph of an SCI participant performing the Romberg balance test. (*C*) Participant balance duration in Romberg test, averaging successive measures within counterbalanced groups of four for each participant with and without feedback (n = 4, 1 male, 3 female, ages 37 to 66; P = 0.004, linear mixed model, H_0: no differences exist in group means). (*D* and *E*) Kinematic analysis of 10-meter walk (10MWT) of Participant P5 using motion pose estimation (male, age 58, stroke patient). (*D*) OpenPose BODY_25 keypoints extracted from the video. The pelvis was selected as the center of the participant for the purpose of tracking. (*E*) Example pelvis-center trajectory for one video shown in normalized units using shoulder–shoulder distance as a reference. (*F* and *G*) Outcomes from 22 walking sessions for Participant P5 (vertical bars, standard deviation; shaded boxes, interquartile range; horizontal lines, medians; filled black circles, group means; colored markers, individual trial outcomes). (*F*) Lateral standard deviation (within-subject n = 22; P = 0.049, Mann–Whitney U test; H_0: no difference with feedback). (*G*) Lateral range (within-subject n = 22; P = 0.12, Mann–Whitney U test; H_0: no difference with feedback).

is possible through the hybrid implementation of a DC haptic motor, which enables 128 degrees of freedom across 64 independently controlled haptic units and two devices. Although the actuators can be fabricated as close as 10 mm by shortening the interconnects, we select a spacing of 17 mm to match the spatial resolution of skin regions outside the hands—including the forearms, 2.4 cm; back, 2.5 cm; and legs, 2.7 cm (two-point discrimination population means) (45, 46). Figs. 3 *F* and *G* show that users reliably discriminate between adjacent nodes at this spacing with high accuracy. Furthermore, users are highly accurate at discriminating between nodes delivering bimodal stimuli when spaced at 2.7 cm. As summarized in *SI Appendix*, Table S1, these capabilities substantially outperform existing alternatives, positioning AR/VR to extend beyond audiovisual experiences with broad impact in entertainment, medicine, and education. Furthermore, the implementation of dual haptic arrays described in this work can be readily expanded to larger networks distributed across the body, limited only by bandwidth of BLE communication.

We demonstrate a high-information-density interface that is particularly well suited to address impaired cutaneous plantar sensation. Smart insoles have been developed over the past decade to monitor gait, identify interventions, and enhance clinical assessments—yet existing systems focus on monitoring and evaluation rather than real-time feedback (47, 48). In contrast, our approach provides continuous haptic feedback with a spatial pattern directed by plantar pressure. As summarized in *SI Appendix*, Table S2, this strategy supports a richer encoding of plantar information, opening possibilities for somatosensory substitution. Importantly, this framework is not limited to custom hardware, and it can be integrated with commercially available insole systems that obtain plantar pressure data in real time, supporting broader translational potential.

Fig. 4 shows that the haptic arrays reliably reproduce spatial patterns of vibration and thermal feedback derived from plantar pressure, and participants are able to perceive differences in these patterns. Clinical participants exhibit lesser overall matching accuracy compared with healthy adults, but their performance remains robust along the heel–toe axis. This is particularly relevant for gait related feedback. CoP analyses indicate that the matching performance of clinical participants is substantially affected by their ability to generate distinct reference patterns. Participants who record closely spaced or overlapping reference snapshots, such as Fig. 4*F*, are effectively evaluated under more challenging discrimination conditions, which may partially explain reduced accuracy. As suggested by outcomes from standard assessments (*SI Appendix*, Table S3), this difficulty in generating distinct plantar pressure patterns may be driven by limitations in muscle control and fatigue during this test.

Along with establishing that users can map between stimulation sites and sensor locations, the pattern-matching tests highlight a potential point-of-care application in physical therapy. Physical and occupational therapy for individuals with stroke and SCI rely

heavily on verbal and visual cueing to promote awareness of posture and gait—cues that can be difficult to perceive when plantar sensation is impaired. For example, an individual with a stroke may be unaware of the asymmetric loading between their affected (somatosensory input likely intact) vs. unaffected (somatosensory input likely impaired) lower extremity. With our system, the clinician can see the true plantar pressure distribution in real time and use it to drive prescribed vibration patterns that cue the participant toward a target posture and weight shift.

In addition to clinician-guided cues, we evaluated the feasibility of using the system to provide vibrotactile feedback directly to participants, without continuous clinician involvement. A key challenge in designing interventions for individuals with somatosensory impairments is the heterogeneity in motor and sensory presentation: Even participants with similar spinal levels of injury following SCI can exhibit markedly different motor and sensory profiles (49, 50). Our system is particularly well suited to overcome this challenge, because the mapping between plantar pressure and haptic feedback is easily reconfigured without altering the underlying hardware. For example, the same hardware can be deployed unilaterally for individuals with stroke or bilaterally for individuals with SCI. As shown in Figs. 3 *F* and *G*, participants discriminate spatial patterns with high accuracy on the forearms, legs, and feet, showing that sensory substitution can potentially be adapted to a wide range of body segments. Fig. 5 illustrates several exploratory case studies demonstrating that individuals can use the device during standing and walking, supporting its feasibility in functional contexts. Overall, these results suggest potential for use outside of clinical settings and during activities of daily living.

Along with promising findings, we acknowledge several limitations of our study. As a feasibility study limited to a small sample size, the present work was not designed to quantify clinical efficacy at the group level or long-term impact on quality of life. Future work will include testing with a larger cohort of clinical participants to validate our device at the group level. Because this was a single-session study with a time allotment similar to a physical therapy visit, feasibility was assessed over a 2-h window. Establishing reliability, stability, and user acceptance beyond 2 h will be important for justifying continuous use over a day of activity. Future work will also help optimize battery life to support operation beyond the 3 h targeted in this study. Finally, since thermal feedback was not tested clinically, our results motivate future long-term experiments into its impact. In the present study, vibrotactile feedback was used to substitute instantaneous plantar pressure during standing and walking feasibility experiments, whereas thermal stimulation is envisioned as a complementary channel for informing long-term behaviors. For example, thermal feedback may be used to guide users away from plantar pressure hotspots that could turn into pressure injuries. The focal loading patterns displayed by Participants P4 (SCI) and P5 (stroke) in Fig. 3*B* illustrate technical capabilities for this approach, although it was not directly tested in the present functional studies.

In summary, interfacing with the skin through a hybrid DC motor strategy, the multimodal haptic platform introduced here offers a compelling approach for engaging the somatosensory system across multiple limbs. Potential use is not limited to individuals with stroke and SCI. Loss of protective sensation is also the strongest risk factor for diabetic foot ulceration, which can lead to lower limb amputation if left untreated (51). For older individuals, loss of plantar sensation amplifies comorbidities such as fall risks (52). For chemotherapy patients, loss of sensation is an early warning sign for damaging neuropathic symptoms (53, 54). Altogether, this work highlights the potential of information-rich cutaneous interfaces to substitute function in plantar sensory impairment, expanding the scope of somatosensory engagement for rehabilitation and future AR/VR experiences.

Materials and Methods

Fabrication of the Haptic Array. The haptic device electronics were assembled on a flexible printed circuit board (PCBWay). A BLE-enabled microcontroller (ISP1807, Insight SiP), integrating the nRF52840 System-on-Chip (Nordic Semiconductor) and an onboard antenna, manages device operation. The system is powered by a 500-mAh rechargeable lithium-ion battery (LP802036JU, Jauch Quartz). Power management circuitry includes a 5.1-V DC–DC boost converter (TPS61235, Texas Instruments) to drive the transducers and a low-dropout regulator (TPS7A0231, Texas Instruments) for logic-level power. A 500-mF supercapacitor (EDLC371420, TDK) stabilizes the 5.1-V output. Each actuator is driven by an independent H-bridge (DRV8837, Texas Instruments), with logic inputs provided through GPIO expanders (TCA9555, Texas Instruments) connected to the controller over a two-wire serial interface. Temperature sensing is performed using negative temperature coefficient thermistors (100 kΩ at 20 °C) and demultiplexed (MAX4691EGE+, Analog Devices) to the integrated analog-to-digital converters of the microcontroller. The device encapsulation comprises a multilayer silicone structure. The exterior top and bottom surfaces consists of a 300-μm silicone-based elastomer layer (Silbione RTV 4420, Elkem) cured at 75 °C for 3 h within a two-part aluminum mold.

Fabrication of the Insole-Based Pressure Sensor Array. The pressure sensor array was developed in Ref. 55. The electronics design includes a DC–DC converter (TPS63802, Texas Instruments), battery-charging IC (MCP73831, Microchip Technology), MOSFET (DMT4011LFG-13, Diodes Incorporated), instrumentation amplifier (INA181, Texas Instruments), and BLE module (BL652-SC-01, Ezurio), along with associated passive components. Force-sensitive material (XactFSR, Sensitronics) is laser-cut into 20 mm (large sensor) or 17 mm (small sensor) disks using a VLS CO_2 laser cutter (2% power, 5% speed, 1,000 pixels-per-inch). The black conductive side of each disk is placed against the interdigitated electrodes with no overlap, then encapsulated using a Kapton-backed adhesive laminated to avoid lateral displacement.

Thermal and Mechanical Characterization. Mechanical measurements were performed using two inertial measurement units (IMUs) capable of triaxial accelerometry and triaxial angular velocity measurements via integrated gyroscopes. The primary IMU was mechanically isolated on an island to capture the device motion, while the secondary IMU, embedded in the sensor body, served as a backup and for potential artifact cancellation. Thermal measurements were conducted using an infrared camera (a6255sc, FLIR Systems) to capture surface temperature distributions during operation.

Sensory Substitution Experiments with Human Participants. All participation was fully voluntary with informed consent obtained before the experiments. Research protocols were approved by the Institutional Review Board at Northwestern University (STU00218277). Foot sensors and haptic receivers were charged and tested before the clinical experiments. The participant was interviewed about the medical problems they are facing due to their condition. The haptic receivers were placed on the participant's arms, and the insoles were placed in the participant's shoes. Insole pads were placed on the insoles to prevent damage. Sleeves were placed on the participant's arms to prevent the receivers from folding onto themselves. The devices were then tested again, and the vibration gain was adjusted to the levels that felt comfortable for the participant.

Evaluation of the Perception of Vibration on Human Participants. The experiment utilized an odd-man-out spatial discrimination task where three successive vibrations (50% duty cycle intensity for 3 s) were delivered to two adjacent actuator locations. The three possible actuator locations were color-coded: green (Pair 1, distal end of the device), yellow (Pair 2, middle of the device), and blue (Pair 3, proximal end of the device). The haptics device was mounted in a sequence of six rounds across various body parts: arm, leg, foot, leg, foot, and arm. In each round, participants (n = 12; 6 male, 6 female; ages 28 to 34) were given cues randomly across the three actuator locations, with each location presented six times in random order. To provide consistent conditions for testing

across multiple body locations, healthy participants were recruited for this task. To maintain blinding and minimize sensory interference, participants were covered with a cape, wearing both earplugs (SA-7-5, Lysian) and noise-canceling headphones (WH-CH720N, Sony). Pink noise was continuously played through the headphones throughout the experiments. The Wilcoxon signed-rank test was used to evaluate statistical significance, given the null hypothesis of random selection between three choices. The experimental setup is illustrated in Fig. 3*E*, raw data are reported in *SI Appendix*, Tables S4–S6, statistical analysis is given in *SI Appendix*, Table S9, and results are plotted in Fig. 3*F*.

Evaluation of the Perception of Heat on Human Participants. The experiment utilized an odd-man-out spatial discrimination task to evaluate thermoreception ($n = 12$; 6 male, 6 female; ages 28 to 34). Participants were presented with three successive thermal stimuli (40 °C for 20 s). The stimuli were delivered by the haptics device to a specific arrangement: a pair of thermal nodes spaced 27 mm apart in the front area of the device. This specific node pair constituted the single tested actuator location. The haptics device was mounted exclusively on the arm. In each round, participants received cues randomly across the single actuator location, with the location being tested six times in random order (for a total of six trials per round, assuming one odd-man-out stimulus delivery constitutes one trial). To maintain blinding and minimize sensory interference, participants were covered with a loose opaque garment, wearing both earplugs (SA-7-5, Lysian) and noise-canceling headphones (WH-CH720N, Sony). Pink noise was continuously played through the headphones throughout the experiments. The Wilcoxon signed-rank test was used to evaluate statistical significance, given the null hypothesis of random selection between three choices. The experimental setup is illustrated in Fig. 3*E*, raw data are reported in *SI Appendix*, Tables S7 and S8, statistical analysis is given in *SI Appendix*, Table S9, and results are plotted in Fig. 3*G*.

Pattern Matching Snapshot Task. Each healthy participant ($n = 12$; 6 male, 6 female; ages 28 to 34) and sensory impaired participant (impaired side, $n = 7$; dominant side, $n = 7$; 3 male, 4 female; ages 35 to 65) was asked to orient their feet by shifting their weight to five different areas shown in Fig. 4*B* (medial toe, lateral toe, arch, medial heel, and lateral heel). Reference recordings of the insole pressure maps and the corresponding patterns of the vibrating receiver were taken for all five areas (Fig. 4*C*). A training stage then followed, in which the five recorded vibrations were played back to the participant, familiarizing them with the test procedure. A mock test was then performed using a previously recorded vibration pattern delivered through the haptic receiver. The snapshot experiment then started: a random sequence of 25 vibrations was played back to the participant, one at a time. The participant was asked to identify the foot orientation that corresponded to each vibration by pointing at the foot chart (Fig. 4*B*). The participant was then asked to orient the pressure on their foot in a way that reproduces the given vibration. Upon doing so, the corresponding pressure map was recorded. The verbal responses and recorded pressure maps were then compared against the reference recordings, and the matching ratios were extracted. CoP analysis was performed according to *SI Appendix*, Fig. S3. We assessed whether the accuracy of clinical and healthy groups were significantly above chance level using the Wilcoxon signed-rank test. The null hypothesis assumed random guessing among five options, corresponding to a chance accuracy of 20%. Raw data are reported in *SI Appendix*, Figs. S4 and S5, statistical analysis is given in *SI Appendix*, Table S10, and results are reported in Figs. 4 *D*–*H*.

Romberg Test with and without Feedback. During this test, the participant was allowed to support themselves using parallel bars. By the discretion of the monitoring clinician, some participants wore a gait belt to mitigate fall risks. The physical therapist would only pull on the belt if the participant had already lost balance. After instruction on the test and devices, the participants ($n = 4$; 1 male, 3 female; ages 37 to 66) would be allowed two trials with and without feedback to train them on the procedure. A trial of the Romberg test was then conducted, in which the participant's ability to balance was evaluated with eyes closed, feet touching heel-to-heel, and arms crossed, pressed against the torso. Each participant would try to maintain their balance, and they were evaluated on the time they could stand without opening their eyes, shifting their feet, or moving their arms. During the experiment, 16 repeated trials were recorded for each participant. To reduce fatigue, the participants were asked to sit and rest for 2 min between every four attempts. The sequence of attempts with feedback and without feedback (one haptic receiver on each forearm) were counterbalanced between rest intervals. Statistical significance for the outcomes of these experiments was evaluated by modeling the presence and absence of feedback as a factor in a linear mixed model (53 degrees of freedom). Ultimately, the *P*-value was determined under the null hypothesis that no differences exist in group means. The experimental setup is pictured in Fig. 5*B*, raw data are reported in *SI Appendix*, Fig. S6, statistical analysis is given in *SI Appendix*, Table S11, results are reported in Fig. 5*C*, and an example pressure-map time-series is given in Movie S1.

10-Meter Walk Test with and without Feedback. One participant was selected to evaluate usability during a 10MWT. A brief training session was conducted in which the participant shifted their weight between toe and heel, holding each position for 1 to 2 s to perceive the vibration. In each trial, the participant initiated gait on a standardized walkway and ambulated forward toward a frontal-view camera positioned at the end of the walkway. Videos were recorded using the rear camera of a Google Pixel 7 smartphone at 30 fps. Because these recordings were acquired during a broader data-collection session, other researchers were occasionally visible in the videos. The participant performed each walk with their eyes closed, and, to mitigate fall risks, the participants wore a gait belt that allowed the attending clinician to support their weight if they lost their balance. The participant performed 24 successive walks. To reduce fatigue, the participants were asked to sit and rest for 2 min between every four attempts. The sequence of attempts with feedback and without feedback (one haptic receiver on each forearm) were counterbalanced between rest intervals. Motion pose estimation was performed according to the approach detailed in *SI Appendix*, *SI Methods*. The experimental setup is illustrated in Fig. 5*D*, raw data are reported in *SI Appendix*, Fig. S7, statistical analysis is given in *SI Appendix*, Table S12, results are plotted in Figs. 5 *F* and *G*, and an example video is given in Movie S2.

Data, Materials, and Software Availability. All study data are included in the article and/or supporting information.

ACKNOWLEDGMENTS. We thank Sensor Medica for loaning their commercial sensor insoles for evaluation of their platform.

Author affiliations: [a]School of Electrical and Computer Engineering, Georgia Institute of Technology, Atlanta, GA 30332; [b]Querrey-Simpson Institute for Bioelectronics, Northwestern University, Evanston, IL 60208; [c]Department of Mechanical Engineering, Northwestern University, Evanston, IL 60208; [d]Max Näder Center for Rehabilitation Technologies and Outcomes Research, Shirley Ryan AbilityLab, Chicago, IL 60611; [e]Department of Biostatistics and Health Data Science, Lehigh University, Bethlehem, PA 18015; [f]Department of Electrical & Computer Engineering, Lehigh University, Bethlehem, PA 18015; [g]PSYONIC, San Diego, CA 92131; [h]Department of Semiconductor Convergence Engineering, Sungkyunkwan University, Suwon 16419, Republic of Korea; [i]Department of Physical Medicine and Rehabilitation, Feinberg School of Medicine, Northwestern University, Chicago, IL 60611; [j]Department of Biomedical Engineering, Northwestern University, Evanston, IL 60208; [k]Department of Materials Science and Engineering, Northwestern University, Evanston, IL 60208; and [l]Department of Neurological Surgery, Feinberg School of Medicine, Northwestern University, Chicago, IL 60611

Author contributions: M.T.F., Y.-T.H., D.S., R.H., S.A., J.C., R.R., J.P., C.B., T.S., M.H., J.H., K.L.B., R.S., S.A.A., F.A.-N., J.-Y.Y., A.A., A.J., and J.A.R. designed research; M.T.F., Y.-T.H., D.S., R.H., S.A., R.R., J.P., C.B., T.S., M.H., J.H., K.L.B., S.A.A., F.A.-N., and A.J. performed research; M.T.F. contributed new reagents/analytic tools; M.T.F., Y.-T.H., C.B., J.T., and R.S. analyzed data; and M.T.F. wrote the paper.

1. L. M. Carey, T. A. Matyas, C. Baum, Effects of somatosensory impairment on participation after stroke. *Am. J. Occup. Ther.* **72**, 7203205100p1–7203205100p10 (2018), 10.5014/ajot.2018.025114.
2. D. Hyndman, A. Ashburn, E. Stack, Fall events among people with stroke living in the community: Circumstances of falls and characteristics of fallers. *Arch. Phys. Med. Rehabil.* **83**, 165–170 (2002).
3. M. Kochman, M. Kasprzak, A. Kielar, The impact of proprioception impairment on gait function in stroke survivors: A comprehensive review. *Front. Neurol.* **16**, 1577919 (2025), 10.3389/fneur.2025.1577919.
4. N. B. Finnerup, I. L. Johannesen, A. Fuglsang-Frederiksen, F. W. Bach, T. S. Jensen, Sensory function in spinal cord injury patients with and without central pain. *Brain* **126**, 57–70 (2003).
5. C. M. Klingner, O. W. Witte, Somatosensory deficits. *Handb. Clin. Neurol.* **151**, 185–206 (2018), 10.1016/B978-0-444-63622-5.00009-7.
6. B. Balaban, F. Tok, Gait disturbances in patients with stroke. *PM&R* **6**, 635–642 (2014).
7. E. Kal *et al.*, How physical therapists instruct patients with stroke: An observational study on attentional focus during gait rehabilitation after stroke. *Disabil. Rehabil.* **40**, 1154–1165 (2018).
8. T. Vachranukunkiet, A. Esquenazi, Pathophysiology of gait disturbance in neurologic disorders and clinical presentations. *Phys. Med. Rehabil. Clin. N. Am.* **24**, 233–246 (2013).
9. G. Abbruzzese, A. Berardelli, Sensorimotor integration in movement disorders. *Mov. Disord.* **18**, 231–240 (2003).

10. T. Kodama, K. Kitai, Clinical usefulness of real-time sensory compensation feedback training on sensorimotor dysfunction after stroke. *Stroke Manag. Pearls* (IntechOpen, 2023), 10.5772/intechopen.111668.
11. M. Yekutiel, E. Guttman, A controlled trial of the retraining of the sensory function of the hand in stroke patients. *J. Neurol. Neurosurg. Psychiatry* **56**, 241–244 (1993).
12. R. Newport, J. V. Hindle, S. R. Jackson, Links between vision and somatosensation: Vision can improve the felt position of the unseen hand. *Curr. Biol.* **11**, 975–980 (2001), 10.1016/S0960-9822(01)00266-4.
13. T. M. Herter, S. H. Scott, S. P. Dukelow, Vision does not always help stroke survivors compensate for impaired limb position sense. *J Neuroeng. Rehabil.* **16**, 129 (2019), 10.1186/s12984-019-0596-7.
14. S. J. Lederman, R. L. Klatzky, Extracting object properties through haptic exploration. *Acta. Psychol.* **84**, 29–40 (1993), 10.1016/0001-6918(93)90070-8.
15. S. J. Bolanowski, G. A. Gescheider, R. T. Verrillo, C. M. Checkosky, Four channels mediate the mechanical aspects of touch. *J. Acoust. Soc. Am.* **84**, 1680–1694 (1988).
16. A. Handler, D. D. Ginty, The mechanosensory neurons of touch and their mechanisms of activation. *Nat. Rev. Neurosci.* **22**, 521–537 (2021), 10.1038/s41583-021-00489-x.
17. D. M. Cain, S. G. Khasabov, D. A. Simone, Response properties of mechanoreceptors and nociceptors in mouse glabrous skin: An in vivo study. *J. Neurophysiol.* **85**, 1561–1574 (2001).
18. W. Lin *et al.*, Super-resolution wearable electrotactile rendering system. *Sci. Adv.* **8**, eabp8738 (2022), 10.1126/sciadv.abp8738.
19. A. Akhtar, J. Sombeck, B. Boyce, T. Bretl, Controlling sensation intensity for electrotactile stimulation in human-machine interfaces. *Sci. Robot.* **3**, eaap9770 (2018).
20. G. Grasso, S. Rosset, H. Shea, Fully 3D-printed, stretchable, and conformable haptic interfaces. *Adv. Funct. Mater.* **33**, 2213821 (2023).
21. E. Leroy, H. Shea, Hydraulically amplified electrostatic taxels (HAXELs) for full body haptics. *Adv. Mater. Technol.* **8**, 2300242 (2023).
22. J. Qi, F. Gao, G. Sun, J. C. Yeo, C. T. Lim, HaptGlove–Untethered pneumatic glove for multimode haptic feedback in reality-virtuality continuum. *Adv. Sci.* **10**, e2301044 (2023).
23. M. Zhu *et al.*, "PneuSleeve: In-fabric multimodal actuation and sensing in a soft, compact, and expressive haptic sleeve" in *Proceedings of the 2020 CHI Conference on Human Factors in Computing Systems* (Association for Computing Machinery, 2020), pp. 1–12.
24. M. T. Flavin *et al.*, Bioelastic state recovery for haptic sensory substitution. *Nature* **635**, 345–352 (2024), 10.1038/s41586-024-08155-9.
25. D. Li *et al.*, Miniaturization of mechanical actuators in skin-integrated electronics for haptic interfaces. *Micros. Nanoeng.* **7**, 85 (2021), 10.1038/s41378-021-00301-x.
26. X. Yu *et al.*, Skin-integrated wireless haptic interfaces for virtual and augmented reality. *Nature* **575**, 473–479 (2019).
27. Y. H. Jung *et al.*, A wireless haptic interface for programmable patterns of touch across large areas of the skin. *Nat. Electron.* **5**, 374–385 (2022), 10.1038/s41928-022-00765-3.
28. J.-H. Kim *et al.*, A wirelessly programmable, skin-integrated thermo-haptic stimulator system for virtual reality. *Proc. Natl. Acad. Sci. U.S.A.* **121**, e2404007121 (2024), 10.1073/pnas.2404007121.
29. M. Park *et al.*, Skin-integrated systems for power efficient, programmable thermal sensations across large body areas. *Proc. Natl. Acad. Sci. U.S.A.* **120**, e2217828120 (2023), 10.1073/pnas.2217828120.
30. J. J. Fleck *et al.*, Wearable multi-sensory haptic devices. *Nat. Rev. Bioeng.* **3**, 288–302 (2025), 10.1038/s44222-025-00274-w.
31. K. Song *et al.*, Pneumatic actuator and flexible piezoelectric sensor for soft virtual reality glove system. *Sci. Rep.* **9**, 8988 (2019), 10.1038/s41598-019-45422-6.
32. N. Takahashi, H. Takahashi, H. Koike, "Soft exoskeleton glove enabling force feedback for human-like finger posture control with 20 degrees of freedom" in *2019 IEEE World Haptics Conference*, (IEEE, 2019), pp. 217–222.
33. M. Gori, G. Cappagli, A. Tonelli, G. Baud-Bovy, S. Finocchietti, Devices for visually impaired people: High technological devices with low user acceptance and no adaptability for children. *Neurosci. Biobehav. Rev.* **69**, 79–88 (2016).
34. Y. Liu *et al.*, Electronic skin as wireless human-machine interfaces for robotic VR. *Sci. Adv.* **8**, eabl6700 (2022).
35. J.-H. Youn *et al.*, Skin-attached haptic patch for versatile and augmented tactile interaction. *Sci. Adv.* **11**, eadt4839 (2025).
36. Y. Huang *et al.*, A skin-integrated multimodal haptic interface for immersive tactile feedback. *Nat. Electron.* **6**, 1020–1031 (2023), 10.1038/s41928-023-01074-z.
37. C.Z.-H. Ma, A.H.-P. Wan, D.W.-C. Wong, Y.-P. Zheng, W.C.-C. Lee, A vibrotactile and plantar force measurement-based biofeedback system: Paving the way towards wearable balance-improving devices. *Sensors* **15**, 31709–31722 (2015).
38. J. Vienneau, J. Bauman, S. Nigg, B. M. Nigg, S. E. Jarvis, Investigating the effects of the SurroGait Rx™ device on postural stability, gait, and MSIS-29 outcomes in people with Multiple Sclerosis. *Biomed. J. Sci. & Tech. Res.* **2**, 2329–2336 (2018).
39. C. Wall, D. Wrisley, L. Oddsson,"Vibrotactile feedback of mediolateral trunk tilt or foot pressure increases locomotor performance in healthy older adults–A pilot study" in *2012 Annual International Conference of the IEEE Engineering in Medicine and Biology Society*, (IEEE, 2012), pp. 6145–6148.
40. L. I. E. Oddsson *et al.*, The effects of a wearable sensory prosthesis on gait and balance function after 10 weeks of use in persons with peripheral neuropathy and high fall risk–The walk2Wellness Trial. *Front. Aging Neurosci.* **12**, 592751 (2020), 10.3389/fnagi.2020.592751.
41. A. Hafström, Perceived and functional balance control is negatively affected by diminished touch and vibration sensitivity in relatively healthy older adults and elderly. *Gerontol. Geriatr. Med.* **4**, 2333721418775551 (2018).
42. E. R. Esposito, H. S. Choi, B. J. Darter, J. M. Wilken, Can real-time visual feedback during gait retraining reduce metabolic demand for individuals with transtibial amputation? *PLoS ONE* **12**, e0171786 (2017).
43. A. Brandt, W. Riddick, J. Stallrich, M. Lewek, H. H. Huang, Effects of extended powered knee prosthesis stance time via visual feedback on gait symmetry of individuals with unilateral amputation: A preliminary study. *J. Neuroeng. Rehabil.* **16**, 112 (2019), 10.1186/s12984-019-0583-z.
44. E. Tütün Yümin, T. Tarsuslu Şimşek, Y. Bakar, Plantar sensation and balance in patients with Type 2 Diabetes Mellitus with and without peripheral neuropathy. *Acta Clin. Croat.* **60**, 191–200 (2021).
45. M. F. Nolan, Quantitative measure of cutaneous sensation. Two-point discrimination values for the face and trunk. *Phys. Ther.* **65**, 181–185 (1985).
46. F. Mancini *et al.*, Whole-body mapping of spatial acuity for pain and touch. *Ann. Neurol.* **75**, 917–924 (2014).
47. J. A. Ramirez-Bautista, J. A. Huerta-Ruelas, S. L. Chaparro-Cárdenas, A. Hernández-Zavala, A review in detection and monitoring gait disorders using in-shoe plantar measurement systems. *IEEE Rev. Biomed. Eng.* **10**, 299–309 (2017).
48. J. Lee *et al.*, Flexible smart insole and plantar pressure monitoring using screen-printed nanomaterials and piezoresistive sensors. *ACS Appl. Mater. Interfaces* **17**, 47153–47161 (2025).
49. J. A. Semrau, T. M. Herter, S. H. Scott, S. P. Dukelow, Examining differences in patterns of sensory and motor recovery after stroke with robotics. *Stroke* **46**, 3459–3469 (2015).
50. M. F. Dvorak *et al.*, Minimizing errors in acute traumatic spinal cord injury trials by acknowledging the heterogeneity of spinal cord anatomy and injury severity: An observational Canadian cohort analysis. *J. Neurotrauma.* **31**, 1540–1547 (2014).
51. G. Sloan, D. Selvarajah, S. Tesfaye, Pathogenesis, diagnosis and clinical management of diabetic sensorimotor peripheral neuropathy. *Nat. Rev. Endocrinol.* **17**, 400–420 (2021), 10.1038/s41574-021-00496-z.
52. J. R. Mahoney, K. Cotton, J. Verghese, Multisensory integration predicts balance and falls in older adults. *J. Gerontol. A Biol. Sci. Med. Sci.* **74**, 1429–1435 (2019).
53. M. Seretny *et al.*, Incidence, prevalence, and predictors of chemotherapy-induced peripheral neuropathy: A systematic review and meta-analysis. *Pain* **155**, 2461–2470 (2014).
54. L. A. Colvin, Chemotherapy-induced peripheral neuropathy (CIPN): Where are we now? *Pain* **160**, S1–S10 (2019), 10.1097/j.pain.0000000000001540.
55. A. Akhtar *et al.*, "A low-cost, open-source, compliant hand for enabling sensorimotor control for people with transradial amputations" in *2016 38th Annual International Conference of the IEEE Engineering in Medicine and Biology Society*, (IEEE, 2016), pp. 4642–4645.